Published in final edited form as:
J Med Chem. 2009 April 23; 52(8): 2317–2327. doi:10.1021/jm801110j.

Potent Inhibitors of Pro-Inflammatory Cytokine Production Produced by a Marine-Derived Bacterium

Wendy K. Strangman[1], **Hak Cheol Kwon**[1], **David Broide**[3], **Paul R. Jensen**[1], and **William Fenical**[1,2,*]

[1]Center for Marine Biotechnology and Biomedicine, Scripps Institution of Oceanography, University of California, San Diego, La Jolla, California 92093-0204 USA

[2]Skaggs School of Pharmacy and Pharmaceutical Sciences, University of California, San Diego, La Jolla, California 92093-0204 USA

[3]Department of Medicine, University of California, San Diego, La Jolla, California 92093-0635 USA

Abstract

Cytokines produced through the Antigen Presenting Cell (APC)–T-cell interaction play a key role in the activation of the allergic asthmatic response. Evaluating small molecules that inhibit the production of these pro-inflammatory proteins is therefore important for the discovery of novel chemical structures with potential anti-asthma activity. We adapted a mouse splenocyte cytokine assay to screen a library of 2,500 marine microbial extracts for their ability to inhibit T_H2 cytokine release and identified potent activity in a marine-derived strain CNQ431, identified as a *Streptomyces* species. Bioactivity guided fractionation of the organic extract of this strain led to the isolation of ten new 9-membered *bis*-lactones, splenocins A-J (**1**–**10**). The new compounds display potent biological activities, comparable to that of the corticosteroid dexamethasone, with IC_{50} values from 2–50 nanomolar in the splenocyte cytokine assay. This study provides the foundation for the optimization of these potent anti-inflammatory compounds for development in the treatment of asthma.

Introduction

Asthma is a disease affecting over 15 million people in the United States. The disease is characterized by airway obstruction, bronchial inflammation, and bronchial smooth muscle hyper-reactivity.[1] Symptoms include characteristic wheezing, shortness of breath or difficulty with breathing, and in the USA, approximately 5,000 patients die from asthma each year. Chronic allergic asthma is a complex disease mediated by a number of cellular processes. In chronic asthma, one of the early cellular events in the pathogenesis of the disease is the stimulation of T_H2 lymphocytes by Antigen Presenting Cells (APCs) such as dendritic cells.[2] Upon activation, T_H2 cells secrete a number of cytokines such as interleukins -4, -5, -9, and -13 that activate cellular and molecular cascades, eventually leading to the asthmatic phenotype.[3] Specifically, the T_H2 cytokine interleukin-5 (IL-5) has been shown to be an activator of eosinophils, bone marrow-derived leukocytes responsible in part for persistent inflammation and airway remodeling seen in patients with chronic asthma.[3] Similarly, another T_H2 cytokine interleukin 13 (IL-13) has been shown to play a critical role in murine models of asthma through its actions on airway smooth muscle and epithelial cells.[4] While inhibition of a single T_H2 cytokine may provide little benefit in the treatment of asthma, compounds that

*CORRESPONDING AUTHOR: William Fenical, Tel: (858) 534-2133, Fax: (858) 534-1318, E-mail : wfenical@ucsd.edu.

suppress the production of multiple cytokines could possess significantly greater therapeutic potential.[5]

Despite advances in understanding of the cellular and molecular mechanisms involved in the pathogenesis of asthma, there have been very few novel drug classes developed. In fact, anti-leukotriene agents, and an anti-IgE monoclonal antibody, are the only new asthma drug classes to be released in the last 20 years.[6] As our knowledge of asthma-related molecular mechanisms increases, novel pathways can be targeted for drug development. Assessing natural product extracts presents an excellent way to probe biological systems with a wide variety of molecules in a relatively high-throughput manner.[7] By focusing even further on previously unexplored, marine microbial secondary metabolites, the chances of discovering a novel small molecule inhibitor are further increased.[8] In the current study, 2,500 marine-derived microbial extracts were screened in a mouse splenocyte assay, which models the APC-T_H2 cell population critically involved in the pathogenesis of allergic inflammation related to asthma.

The whole culture extract of a marine-derived actinomycete strain, culture # CNQ431, identified as a *Streptomyces* sp., displayed significant biological activity in the mouse splenocyte assay (IC_{80} = 21 μg/mL for the crude extract) and was therefore targeted for further investigation. This bacterial strain was isolated from oceanic bottom sediments at 30 m depth roughly one mile off the coast of the Scripps Institution of Oceanography in La Jolla, California. Bioactivity guided fractionation and final purification of the cytokine inhibitors from this strain led to the discovery of a new set of bioactive molecules, the splenocins A-J (**1–10**, Figure 1.). These molecules display potent suppression of cytokine production in ranges from low micromolar to low nanomolar and exhibit minimal mammalian cell cytotoxicity, which is only evident at levels in the low molar to high micromolar range. These data indicate a therapeutic ratio in this assay of over 200 with some metabolites, and over 500 in the case of compound **2**. Further biological investigation revealed that all of these molecules not only inhibited the production of T_H2 cytokines IL-5 and IL-13, but also the production of the dendritic cell-associated cytokines IL-1 and TNF-α, indicating immunosuppressive effects on both the APCs (i.e. dendritic cells) and the T_H2 cells.

Compounds **1–10** are characterized by a central nine-membered cyclic *bis*-lactone core. An *N*-formylamino salicylic acid moiety is positioned at C-3′ via an amide bond in all members. This fundamental structure, together with the cyclic *bis*-lactone core, is also seen in molecules of the antimycin class.[9–11] The splenocins are further characterized and differentiated from the antimycins by the presence of benzyl groups positioned at C-7 (**1–3, 10**) and benzoyl groups at C-8 (**4–8**) of the *bis*-lactone ring. Compound **9** contains aromatic functionalities at both the C-7 and C-8 positions. In addition to the benzyl group at C-7, compound **10** contains a hydroxyl group at C-8 instead of the ester functionality seen in splenocins A-I. This hydroxyl functionality can also be seen in other previously described 8-hydroxy antimycins which contain alkyl chains at the C-7 position and differ from each other by the number of carbons in the chain.[12] Representative members of this group, which include deisovalerylblastmycin (C_4 alkyl chain)[13] (**11**), the urauchimycins (C_5)[14] (**12**), and kitamycins (C_6)[15] (**13**) were also isolated from the culture broth of *Streptomyces* strain CNQ431.

Compounds **1–9** displayed low nanomolar activity in the suppression of cytokine production by OVA stimulated splenocytes, similar to that we have observed with the corticosteroid drug dexamethasone. Currently, corticosteroids are the most potent anti-inflammatory drugs on the market. Compound **10** exhibited low micromolar activity in the splenocyte assay. In this paper, we describe the isolation, structure elucidation, and structure activity relationships of the splenocins in the *in vitro* mouse splenocyte assay.

Results

Structure Assignments for the Splenocins

Compound **1** was isolated as an optically active amorphous white powder, which displayed strong IR bands at 3381 and 1748 cm^{-1}, indicating the presence of hydroxyl and carbonyl functional groups. A molecular formula of $C_{26}H_{28}N_2O_9$ was assigned based on interpretation of HR ESI-TOF MS data (Obsd $[M+Na]^+$ at *m/z* 535.1683). Together with the molecular formula and information derived from interpretation of spectral data, several substructures were assembled based on analyses of 1D and 2D NMR experiments (Figure 2; Table 1.).

The first substructure (Figure 2A) was assembled starting with the methine proton H-3 (δ_H 5.24), which showed ^{1}H-^{1}H COSY NMR correlations to both H-4 (δ_H 5.60) and a secondary amide proton (δ_H 6.98). Proton H-4 showed an additional correlation to a methyl doublet (δ_H 1.16). Similarly, a second spin system was assembled starting with oxygenated methine proton H-9 (δ_H 5.01), which showed ^{1}H-^{1}H COSY NMR correlations to a methyl doublet (δ_H 1.32) and H-8 (δ_H 5.19). Proton H-8 showed a further correlation to H-7 (δ_H 2.90), which showed correlations to two methylene protons H1-1″a and H1″b (δ_H 2.97 and 2.71) in the ^{1}H-^{1}H COSY NMR spectrum. HMBC NMR correlations from H-4 and H-7 to carbonyl carbon C-6 (δ_c 172.8) and protons H-3 and H-9 to carbon C-2 (δ_c 170.0) allowed the fragments to be assembled into a nine-membered *bis*-lactone. The orientations of the ester bonds within the *bis*-lactone ring were determined by ^{1}H and ^{13}C chemical shift analysis, and in particular the proton shifts of H-4 and H-9.

A second substructure (Figure 2B) was assembled starting with a downfield resonance (δ_H 8.48) that correlated to the carbon at δ_c 159.1. This shift was explained by a ^{1}H-^{1}H COSY NMR correlation from the formamide proton to an amide proton (δ_H 7.87), which indicated the presence of an *N*-formyl amino group. Next, ^{1}H-^{1}H COSY NMR correlations between aromatic protons H-4′ (δ_H 8.52), H-5′ (δ_H 6.89), and H-6′ (δ_H 7.20) and HMBC correlations from these aromatic protons to quaternary carbons C-1′ (δ_C 112.5) and C-3′ (δ_C 127.7) and hydroxyl-substituted C-2′ (δ_C 150.6) allowed us to assemble a trisubstituted aromatic ring. An HMBC NMR correlation from the amide proton of the *N*-formyl amino group to the aromatic quaternary carbon C-3′ allowed the two pieces to be connected, thereby forming the *N*-formyl-amino salicylic acid moiety as a second substructure. Finally, interpretation of ^{1}H-^{1}H COSY correlations allowed a mono-substituted benzene ring to be defined (Figure 2C). In addition, the methyl singlet, H_3-2‴ (δ_H 2.04, δ_C 20.9), showed an HMBC correlation to carbonyl carbon C-1‴ (δ_C 170.2) defining a single acetate unit (Figure 2D).

The connectivity between the substructures was achieved by interpretation of HMBC NMR correlation data (Figure 2E). The aromatic proton H-6′ showed a C-H long-range correlation to a carbonyl carbon at δ_C 169.5. Both H-3 and the secondary amino proton adjacent to H-3 in the cyclic *bis*-lactone also showed C-H long range correlations to this carbonyl, thereby allowing the *N*-formyl amino salicylic acid substructure to be connected to the *bis*-lactone ring via an amide bridge between C-1′ and C-3. This *bis*-lactone core substructure is the same as that seen in the antimycins, which are characterized by the presence of a C-7 alkyl and C-8 acyl unsaturated hydrocarbon chains[9–11] and in the 8-hydroxy antimycins, deisovalerylblastmycin,[13] urauchimycins,[14] and kitamycins.[15] Additional C-H long range correlations allowed the benzyl substituent to be connected to C-7 of the *bis*-lactone. Further, an HMBC NMR correlation from H-8 to the C-1‴ carbonyl carbon allowed the acetate unit to be connected to C-8, thereby completing the planar structure for **1** (Figure 2E).

The structures of **2** and **3** are very similar to that of **1** in that they contain a benzyl group positioned at C-7 (Table 1). However, they differ from **1** in the length of the acyl chain at C-8.

The length and branching of the side-chains in **2** and **3** were defined by a combination of HRMS and proton NMR analysis.

Similar to compounds **1–3**, compounds **4–8** (Table 2) also possess ester functionalities positioned at C-8. However, for this subset of compounds, HMBC analysis showed correlations from the C-8 ester carbonyl to protons on a second aromatic ring H-3‴ (δ_H 8.04) and H-7‴ (δ_H 8.04), suggesting that these molecules contained a benzoyl group at C-8 rather than an acyl chain (Table 2). In further contrast to **1–3**, compounds **4–8** possess alkyl chains originating at C-7 rather than the corresponding benzyl moieties of **1–3**. The C-7 alkyl chains of **4–8** were assembled based on analysis of HRMS and proton NMR spectroscopic data.

Compound **9** is unique in that it contains aromatic groups at both C-7 and C-8 (Table 3). Similar to **1–3**, the benzyl group at C-7 in **9** was connected to the *bis*-lactone by the observation of COSY NMR correlations from H-7 to H-1″a and H-1″b, and by analysis of HMBC NMR correlations from H-7 to the quaternary aromatic carbon C-2″ and from H-3″ to C-1″. As was observed in compounds **4 – 8**, HMBC NMR correlations were observed from both H-8 and H-3‴ to the C-1‴ ester carbon (δ_c 165.3).

Compound **10** contains the same benzyl functionality at C-7 as in **1–3**, and **9** (Table 3). However, unlike any of the other splenocins, the proton at C-8 (δ_H 3.73/δ_c 77.3) in **10** showed a ^{1}H-^{1}H COSY NMR correlation to a hydroxyl proton, indicating the presence of a secondary alcohol at C-8 rather than an ester. This C-8 hydroxyl group is also shared by the known compounds **11**, [13] **12**, [14] and **13**, [15] which contain C_4, C_5, and C_6 alkyl chains, respectively, at C-7 of the *bis*-lactone ring. Additionally, we isolated compound **14**, a new member of the 8-hydroxy antimycin subset of molecules. Analysis of 1D and 2D NMR spectral data, combined with mass spectral fragmentation information, showed that **14** contains a C-4 branched C_7 alkyl chain originating from C-7 (Supporting Information).

Also isolated from the extract of *Streptomyces* sp., strain CNQ431, were three known derivatives, antimycins A_{6a}, A_{4a} and A_{7a} (**14, 15**, and **16**). As antimycin structures differ from each other by the length and branching of their alkyl and acyl chains, their structures were determined through interpretation of HRMS and by comparison to reported ^{1}H NMR data.[9–11]

Relative Configurations of the Splenocins

The relative configurations of the splenocins were assigned by interpretation of proton NMR coupling constants and by analysis of NOESY NMR data (Table 4 and Figure 3, respectively). On the side of the *bis*-lactone containing the *N*-formylamino salicylic acid group, protons H-3 and H-4 were coupled with coupling constants of 7.0 and 7.5 Hz (Table 4). While this value is suggestive of a *syn* configuration, the coupling constant is not small enough to be definitive.[10] To further support this assignment, NOE NMR correlations were also analyzed. The methyl protons at C-4 showed strong NOE correlations with the secondary amide proton connected to C-3 and a very weak correlation to H-3, while H-3 and H-4 showed strong NOESY correlations to each other. Additionally, there was no apparent NOE correlation between H-4 and the secondary amide proton. Taken together with the coupling constant data, this indicated that H-3 and H-4 were in the *syn* configuration although not quite eclipsed. (Figure 3).

On the opposite side of the ring, the coupling constants between H-7 and H-8, and between H-8 and H-9, are between 9 and 10.5 Hz, which is strong evidence for the assignment of an *anti* configuration. These coupling constants are also consistent with those observed in the antimycin *bis*-lactone ring (Table 4). NOE correlations were analyzed to further confirm this configuration. The methyl protons at C-9 showed strong NOE NMR correlations to H-8. Proton H-9 showed a strong NOE correlation to H-7, and H-7 showed a strong NOE correlation to a

proton in the benzyl ring at C-7, indicating they are in close proximity on the bottom face of the molecule. All splenocins showed similar NOE NMR correlations between protons in the *bis*-lactone ring and displayed similar coupling constants, thereby indicating that they share identical relative configurations (Table 4).

For those compounds possessing a benzyl group at C-7 (**1–3, 9, 10**), a strong NOE NMR correlation was observed between H-8 and H-1″a and a weaker NOE correlation between H-8 and H-1″b, which when combined with the NOE correlation between H-7 and the benzyl at C-7, indicated the spatial orientation for the benzyl functionality (Figure 3). In compound **10**, a further NOE correlation was observed between a proton on the benzyl ring at C-7 and the methyl attached to C-4 on the opposite side of the *bis*-lactone ring, thereby offering evidence relating the configurations of the two halves of the *bis*-lactone ring. Additional NMR-based evidence for this connectivity for **10**, and also for the other benzyl-containing compounds **1–3** and **9** comes from proton chemical shift analysis of the methyl group at C-4. In the splenocins that contain a benzyl group at C-7, the methyl protons at C-4 are shifted upfield roughly 0.2 ppm (from 1.32 ppm to 1.15 ppm) relative to those of the non-benzylated compounds **4–8** (Table 1,Table 2, and Table 3). This upfield shift, combined with the NOE correlation seen in **10**, suggests that the methyl protons at C-4 are being shielded by the adjacent benzyl group at C-7.

Absolute Configurations of the Splenocins

The availability of the secondary alcohol at C-8 made compound **10** an appropriate candidate for absolute configuration determination. The absolute configuration of C-8 in **10** was thus defined by application of the modified Mosher NMR method.[16] Compound **10** was treated with (*R*)-(-)-α-methoxy-α-(trifluromethyl) phenylacetyl chloride (*R*-MTPA-Cl) and (*S*)-(+)-MTPA-Cl in separate experiments. Initially, and quite unexpectedly, the reaction yielded mono-*S*-Mosher and mono-*R*-Mosher amides, respectively, at the 3′-aminophenyl position. The creation of this Mosher amide can be explained through an acyl transfer mechanism in which the formyl group is first displaced by DMAP forming an aniline (Scheme 1.). This group then attacks the Mosher-DMAP conjugate resulting in the Mosher-amide. While this reaction is unprecedented under these conditions, similar deformylation reactions of aromatic *N*-formyl groups have been shown to occur upon heating, or under strongly acidic or strongly basic conditions.[17–19] It would be interesting to investigate this mechanism in greater detail to determine whether it is specific to the splenocins or whether it can be applied more generally to other types of *N*-formyl containing compounds.

Allowing the reaction to proceed longer produced the di-*S*-Mosher product **10a** and di-*R*-Mosher product **10b** respectively, with the second Mosher ester addition at the aromatic hydroxyl position of the *N*-formyl amino salicylic acid moiety (Figure 4a). Continuation of the reaction finally produced the tri-*S* Mosher product **10c** and the tri-*R* Mosher product **10d** with the third ester product at the desired C-8 alcohol position (Figure 4b). However, initial analysis of the tri-Mosher products gave inconclusive stereochemical results. Specifically, subtraction of NMR shifts of the tri-*R*-Mosher product from the tri-*S*-Mosher product following the modified Mosher method protocol gave a negative value (−0.01) for 9-Me and a positive value (+ 0.01) for H-9 on the same side of the Mosher ester at C-8, as well as positive values for H-7 (+ 0.01) and H-1 ″a (+ 0.04) (Figure 4b). Suspecting that the ambiguous data were due to anisotropic effects of the phenyl groups from the Mosher products at the 3′-amine and the 2′ positions, it was reasonable to subtract the ^{1}H NMR chemical shift differences of the di-Mosher products **10a** and **10b** ($\Delta\delta_{diS\text{-}diR}$) from the differences of the tri-Mosher products **10c** and **10d** ($\Delta\delta_{triS\text{-}triR}$, Figure 4c). Analysis of these chemical shift differences ($\Delta\delta_{S(tri\text{-}di)\text{-}R(tri\text{-}di)}$) gave negative values for the methyl protons at -C-9 (− 0.02) and H-9 (− 0.01), and positive

values for protons at H-7 (+ 0.01) and H-1″a (+ 0.04), thus suggesting the absolute configuration at C-8 is *R*.

Since not all splenocins displayed NOE NMR correlations between the left and right side of the *bis*-lactone ring as was seen for compound **10**, it was important to determine the absolute configurations of C-3 and C-4 of the embedded threonine molecule of the *bis*-lactone ring in order to assign the absolute configuration for the entire molecule. Given the *syn* relative configuration between H-3 and H-4 within the constraints of the *bis*-lactone ring system, the D and L isomers of threonine would give opposite configurations within the molecule (Figure 5). To determine whether the threonine moiety was D or L, we performed an acid-catalyzed hydrolysis of **10** followed by derivatization with Marfey's reagent and subsequent Marfey's analysis.[20, 21] Based on the retention time of the derivatized splenocin-derived threonine, relative to derivatized standards, we were able to determine that the threonine component of the *bis*-lactone ring had the L configuration, thereby confirming the complete absolute configuration for **10**. Similar experiments were performed with compound **6** to confirm that both benzyl and benzoyl containing splenocins contained L-threonine in the 3 and 4 positions of the *bis*-lactone ring.

Since only compound **10** was a feasible candidate for Mosher's analysis, we used a series of circular dichroism (CD) spectral comparisons to confirm the absolute configurations of the related compounds **1–9** (Supporting Information). Comparisons of splenocin CD spectra allowed us to group the splenocins into two different CD spectral categories (Figure 6). Compounds **1–3** and **10** displayed a weak absorption at λ 220 nm. Compounds **4–9** comprise the second group, possessing a negative Cotton effect at λ 240 nm and corresponding positive Cotton effect at λ 225 nm (Figure 6 and Supporting Information). Based upon the strong similarities in their CD spectra, it can be assumed that **4–9** all have the same absolute configurations.

As the negative Cotton effect seen in Compounds **4–9** is only observable in compounds containing the C-8 benzoyl group, it is likely that this Cotton effect is due to Exciton Coupling of the 8-*O*-benzoyl group with the 3'-*N*-formyl amino salicylic acid moiety (Figure 7A). In applying the rules for Exciton Coupling of two chromophores, we analyzed three dimensional representations of **4–9** to estimate angular orientations of the electronic transition dipole moment vectors for both the 8-*O*-benzoate and the 3'-*N*-formyl amino salicylamide (Figure 7).[22] The resulting vectors were in accordance with the observed CD spectral data supporting our absolute configuration assignment.

To further confirm the absolute configurations of **4–9**, we performed benzoylation reactions on Compounds **9** and **10**, whose absolute configurations had already been established chemically. These reactions created identical tri-benzoylated products (**9b** and **10g**, Scheme 2). The CD spectra for these two compounds proved to be identical, displaying a negative cotton effect at 235 nm and a corresponding positive signal at 213 nm. Since the absolute configuration of **10** had already been determined through Mosher's and Marfey's analyses, it can now be unambiguously assumed that **9** also shares this configuration. Further, as the initial set of CD experiments showed that **4–9** all have nearly identical Cotton effects, it is reasonable to assume that they all have the same absolute configuration as compound **10**.

A similar set of benzoylation reactions was also performed with compounds **1–3** in an attempt to add an additional chromophore on the salicylic acid (Figure 7) and create Exciton Coupling with the C-7 benzyl group. These products were obtained, but they yielded no observable change in the Cotton effects of their CD spectra and so a different technique was needed. Due to their close structural similarity to compound **10**, we measured their optical rotation values, $[\alpha]_D$, to determine if they share identical absolute configurations. Compounds **2** and **10** both

showed positive optical rotations ($[\alpha]_D$+ 68.0 and $[\alpha]_D$ + 69.6 respectively). These data, combined with the similarities of the CD spectra, provide strong evidence that **1–3** have the same absolute configurations as compounds **4–10**. The results of these experiments confirm that compounds **1–10** all share the same absolute configuration, 3*S*, 4*R*, 7*R*, 8*R*, and 9*S*, which is identical with that of the stereocenters reported for the *bis*-lactone ring of the antimycins.[23]

In vitro Biological Evaluation of Splenocins

The splenocins show potent biological activities in an *in vitro* mouse model of allergen induced T_H2 splenocyte cytokine production characteristic of allergic asthma. As mentioned above, the parent *Streptomyces* strain CNQ431 was selected for further investigation due to the low μg/mL non-cytotoxic inhibition of OVA stimulated splenocyte cytokine interleukin 5 (IL-5) production seen from the crude extract. In pure form, compounds **1–9** showed low nanomolar suppression of IL-5 production, while compound **10** showed inhibition in the low micromolar range (Table 5). The inhibitory activities of **1–10** are comparable to that of the corticosteroid drug dexamethasone at similar nanomolar concentrations (Figure 8). Currently, corticosteroids are the most potent suppressors of cytokine production in asthma. Both dexamethasone and compound **2** inhibit antigen induced IL-5 production levels by greater than 80% of the levels of OVA stimulated control splenocytes. The inhibitory levels of dexamethasone- and **2**-treated cells are comparable to the production levels measured in unstimulated splenocytes.

To determine whether the splenocins inhibited other T_H2 cytokines in addition to IL-5, levels of the T_H2 cytokine IL-13 were also analyzed in the splenocyte cultures (Table 5). These data indicated that compounds **1–10** inhibit multiple T_H2 cytokines including IL-5 and IL-13 at low ng/mL concentrations *in vitro*.

Since the splenocyte cell culture population is a heterogeneous mixture of cell types, we were interested in determining whether splenocins were acting solely on T_H2 cells or if they also inhibited the cytokine production capabilities of APCs. To investigate this, we quantified cytokine levels of the APC-derived cytokines IL-1 and TNF-α. These studies demonstrated that the splenocins are capable of inhibiting both T_H2 and APC derived cytokines (Figure 9). Compounds **2** and **7** inhibited IL-1 by approximately 85% and TNF-α by approximately 75% relative to the OVA stimulated control cells. Compounds **2** and **7** are as effective as dexamethasone in inhibiting T_H2 cytokine production and are only slightly less effective than dexamethasone in suppressing APC cytokine production of IL-1 and TNF-α.

Due to the structural similarity of the splenocins to the known antimycins, compound **17** (Sigma) was also tested in this assay. Antimycin A_2, which has a hexyl alkyl chain at C-7 and a propyl acyl chain at C-8, displayed a similar activity profile to that seen from the splenocins (data not shown). A recent paper reports that antimycins induce cellular apoptosis in hepatocytes by binding to the hydrophobic groove of Bcl-2/Bcl-x_L proteins on the surface of mitochondria.[24] However, these studies also report cell death in the micromolar ranges and similar experiments with lymphocytes or splenocytes have not been reported. Recently reported studies with antimycins have also shown that at concentrations lower than the cytotoxic threshold, immunosuppressive anti-cancer activities are observed. Specifically, *in vivo* cancer models explored by Nose and co-workers have shown non-toxic inhibition of angiogenesis and HIF-1α inhibition by antimycins at concentrations similar to those used in our investigations.[25] Another recent *in vivo* study investigated the non-toxic cardio-protective effects of antimycin in combating ischemia, while *in vitro* studies have examined the non-toxic effects of antimycins in mouse hepatocytes.[26] To our knowledge, the present study reflects the first investigations of the novel splenocins and the structurally related antimycins in a model of allergic inflammation.

The splenocyte assay we have utilized provides a novel assay to screen natural product libraries for compounds with the ability to inhibit pro-inflammatory cytokines produced by the antigen-presenting cell T-cell interaction. By using corticosteroids as our control therapy, we are able to compare the anti-inflammatory potency of novel compounds to the most potent anti-inflammatory molecules in clinical use today. Interestingly, in this study we have identified a series of new compounds **1–9**, that display potency levels equal to those of the corticosteroid dexamethasone. As corticosteroids are currently the most effective therapy in asthma, identifying new compounds that have potent anti-inflammatory activities, but do not have the same negative side effects associated with corticosteroid therapy, would be an important therapeutic advance.

While further immunological experiments are in preparation to further investigate this activity using the mouse allergic asthma model *in vivo*, our initial data suggests a potential for therapeutic development of a splenocin-derived drug for inflammatory diseases such as asthma, as well as their potential uses as anti-inflammatory agents in other diseases in which suppression of cytokine production by APCs and T-cells may be beneficial.

Experimental Section

General Experimental Procedures

^{1}H, ^{13}C, and 2D NMR spectral data were obtained on Varian Inova 300 MHz and 500 MHz NMR spectrometers. UV spectra were recorded on a Varian Cary 50 Conc UV Visible spectrophotometer with a path length of 1 cm. IR spectra were recorded in a Nicolet IR100 FT-IR spectrometer. Optical Rotations were measured using a Rudolph Research Autopol III Automatic polarimeter with a 10 cm cell. High resolution MALDI-FTMS data were collected on an IonSpec Ultima mass spectrometer at the Scripps Research Institute, La Jolla. Low resolution LC/MS data were obtained on a Hewlett-Packard series 1100 LC/MS system with a reversed phase C18 column (Agilent, 4.6 mm × 100 mm, 5 μm) with a 0.7 mL/min flow rate. CD Spectra were obtained on a Jasco 810 spectropolarimeter with a 1 cm path length. CD spectra were also recorded using an AVIV Instruments Inc. model 215 circular dichroism Spectrometer. OD measurements of ELISA experiments were recoded at 450 nm on a Biorad Model 680 microplate reader. The purity of all new natural products (**1–10**) was assessed by analytical HPLC using either silica gel (normal phase) or C-18 reversed phase columns. HPLC traces, indicating high purity (ca. 95% or greater) for **1–10**, are found in the supporting information.

Isolation of CNQ431 Strain, Identification, Cultivation, and Extraction

Marine-derived *Streptomyces* strain CNQ431 was isolated using growth medium A1+C (10 g of starch, 4 g of peptone, 2 g of yeast extract, 1 g of calcium carbonate, 18 g of agar, and 1 L of seawater) from a marine sediment collected from a depth of 30 m 1 mile Northwest of the Scripps Institution of Oceanography (La Jolla, CA). Strain CNQ431 was classified as a *Streptomyces* sp. based on 16S rDNA analysis which showed 100% sequence identity between strain CNQ431 and 5 strains including *Streptomyces fungicidus*, strain AY636155; two strains of an unidentified *Streptomyces*, strains AF429400 and AM21770.1; and two identified strains of bacteria in the family Streptomycetaceae, AY944261 and AY944255. The strain was cultured in 60 × 1 L volumes of media A1 while shaking at 230 rpm for 3 days. After 72 hours, 20 g/L of XAD-7 adsorbent resin was added to each flask and the flasks were allowed to shake for an additional 24 hours. At this time, an additional 20 g/L of XAD-7 adsorbent resin was added. The cultures were allowed to shake for an additional 24 hours, at which time the resin was collected by filtration through cheesecloth, washed with deionized water and eluted twice with acetone. Evaporation of the acetone *in vacuo* left a wet residue that was partitioned with EtOAc, providing 130 mg of dry organic extract per 1 L of culture after solvent removal.

Isolation and Purification of Compounds 1–10

The EtOAc extract of a 60 × 1 L fermentation (7.0 g) was subjected to silica gel column chromatography purification eluting with solvent mixtures of *n*-hexanes-EtOAc (10:1), *n*-hexanes-EtOAc (5:1), *n*-hexanes-EtOAc (2.5:1), *n*-hexanes-EtOAc (1:1), EtOAc, EtOAc – MeOH (10:1), and 100% MeOH, successively. The EtOAc – MeOH (2.5:1) and EtOAc – MeOH (1:1) eluting fractions (labeled Q431-3 and 4) showed the most potent IL-5 inhibition levels in the mouse splenocyte assay, and by LCMS, contained **1–9** as well as several antimycins. The 100% EtOAc (CNQ431-5) fraction contained **10** as well as several 8-hydroxy antimycins. Fractions CNQ-431-3,4, and 5 were re-fractionated by C-18 reversed-phase HPLC with an MeCN-H_2O step gradient from 40% MeCN to 100% MeCN over 110 min. to obtain nearly pure **1–10**. Final purification was performed by C-8 and C-18 reversed-phase column chromatography with isocratic solvent systems ranging between 50:50 and 90:10 MeCN:H_2O.

Compound 1

White amorphous powder, 2 mg, CD (MeCN) $\Delta\varepsilon_{220}$ +2.5, $\Delta\varepsilon_{190}$ −4.8; UV (EtOH): 230 (ϵ = 23,000), 360 (ϵ = 5,750) nm. IR (film) ν_{max} 3381, 1748, 1527, 1368, and 736 cm^{-1}. HR ESI TOF MS: Obsd *m/z* 535.1683 $[M+Na]^+$ ($C_{26}H_{28}N_2O_9Na$ requires 535.1687). See Table 1 for NMR data.

Compound 2

White amorphous powder, 6 mg, $[\alpha]_D$ = + 68 (0.1, CH_3OH); CD (MeCN) $\Delta\varepsilon_{213}$ +4.2, $\Delta\varepsilon_{190}$ −10.8; UV (EtOH): 230 (ϵ = 18,000), 320 (ϵ = 4,300) nm. IR (film) ν_{max} 3361, 1746, 1527, 1369, and 737 cm^{-1}. HR ESI TOF MS: Obsd *m/z* 541.2167 $[M+H]^+$ ($C_{28}H_{33}N_2O_9$ requires 541.2180). See Table 1 for NMR data.

Compound 3

White amorphous powder, 2 mg, CD (MeCN) $\Delta\varepsilon_{220}$ +4.4, $\Delta\varepsilon_{190}$ −7.0; UV (EtOH): 230 (ϵ = 19,400), 320 (ϵ = 4,400) nm. IR (film) ν_{max} 3381, 1747, 1527, 1355, and 744 cm^{-1}. HR ESI TOF MS: Obsd *m/z* 555.2322 $[M+H]^+$ ($C_{29}H_{35}N_2O_9$ requires 555.2337). See Table 1 for NMR data.

Compound 4

White amorphous powder, 2 mg, CD (MeCN) $\Delta\varepsilon_{238}$ −2.2, $\Delta\varepsilon_{220}$ +2.3; UV (EtOH): 230 (ϵ = 16,400), 320 (ϵ = 3,000) nm. IR (film) ν_{max} 3361, 1740, 1537, 1350, and 702 cm^{-1}. HR ESI TOF MS: Obsd *m/z* 511.1716 $[M-H]^-$ ($C_{26}H_{27}N_2O_9$ requires 511.1722). See Table 2 for NMR data.

Compound 5

White amorphous powder, 2 mg, CD (MeCN) $\Delta\varepsilon_{237}$ −2.9, $\Delta\varepsilon_{221}$ +4.0; UV (EtOH): 230 (ϵ = 18, 400), 320 (ϵ = 3,300) nm. IR (film) ν_{max} 3381, 1753, 1534, 1345, and 737 cm^{-1}. HR ESI TOF MS: Obsd *m/z* 541.2168 $[M+H]^+$ ($C_{28}H_{31}N_2O_9$ requires 541.2180). See Table 2 for NMR data.

Compound 6

White amorphous powder, 2 mg, CD (MeCN) $\Delta\varepsilon_{241}$ −2.2, $\Delta\varepsilon_{220}$ +4.5; UV (EtOH): 230 (ϵ = 21,100), 320 (ϵ = 4,400) nm. IR (film) ν_{max} 3347, 1760, 1540, 1369, and 744 cm^{-1}. HR ESI TOF MS: Obsd *m/z* 555.2326 $[M+H]^+$, ($C_{29}H_{35}N_2O_9$ requires 555.2337). See Table 2 for NMR data.

Compound 7

White amorphous powder, 2 mg, CD (MeCN) $\Delta\varepsilon_{239}$ −2.1, $\Delta\varepsilon_{221}$ +2.8; UV (EtOH): 230 (ϵ = 22,700), 320 (ϵ = 5,700) nm. IR (film) ν_{max} 3347, 1740, and 764 cm^{-1}. HR ESI TOF MS: Obsd *m/z* 569.2481 $[M+H]^+$ ($C_{30}H_{37}N_2O_9$ requires 569.2493). See Table 2 for NMR data.

Compound 8

White amorphous powder, 7 mg, CD (MeCN) $\Delta\varepsilon_{240}$ −10.3, $\Delta\varepsilon_{221}$ +14.9; UV (EtOH): 230 (ϵ = 23,000), 320 (ϵ = 6,000) nm. IR (film) ν_{max} 3315, 1725, 1534, 1275, 785 cm^{-1}. HR ESI TOF MS: Obsd *m/z* 583.2664 $[M+H]^+$ ($C_{31}H_{39}N_2O_9$ requires 583.2577). See Table 2 for NMR data.

Compound 9

White amorphous powder, 5 mg, CD (MeCN) $\Delta\varepsilon_{238}$ −4.5, $\Delta\varepsilon_{217}$ +3.9; UV (EtOH): 230 (ϵ = 23,000), 350 (ϵ = 5,750) nm. IR (film) ν_{max} 3374, 1744, 1535, 1370, and 734 cm^{-1}. HR ESI TOF MS: Obsd *m/z* 575.2000 $[M+H]^+$ ($C_{31}H_{31}N_2O_9$ requires 575.2024). See Table 3 for NMR data.

Compound 10

White amorphous powder, 6 mg, $[\alpha]_D$ = +70 (*c* 0.18, CH_3OH). UV (EtOH): 230 (ϵ = 29,600), 337 (ϵ = 5,600) nm. IR (film) ν_{max} 3375, 1740, 1540, 1360, and 730 cm^{-1}. HR ESI TOF MS: Obsd *m/z* 493.1573 $[M+Na]^+$ ($C_{24}H_{26}N_2O_8Na$ requires 493.1581). See Table 3 for NMR data.

Mosher MTPA esters 10a/10b, 10c/10d, 10e/10f

Compound **10** (1.0 mg) was divided into two equal portions and each was dissolved in 500 μL of pyridine in separate reaction vials. To each, 5 mg of DMAP and either 10 μL of (R)-MTPA-Cl or 10 μL of (S)-MTPA-Cl was added. After 5 hours, LC-MS analysis indicated that equal amounts of di- and tri-Mosher ester products were formed. The reaction was terminated and reaction products were purified by C-18 reversed phase HPLC. The ^1H NMR spectra for the (*R*)-MTPA-Cl and (*S*)-MTPA-Cl di- and tri-Mosher esters were recorded (see Supporting Information for NMR data).

Benzoylation of Compounds 9 and 10 to yield 9b and 10g

Compounds **9** and **10** (0.5 mg each) were dissolved in separate 1.0 mL volumes of pyridine. To each sample, DMAP 5 mg and benzoyl chloride (1 mg) were added and the reaction was allowed to proceed for 12 hours. The reaction mixture was filtered and concentrated under reduced pressure. The resulting benzoylated products **9b** and **10g** were purified by C-18 HPLC and analyzed by LC-MS. LRMS (ESI) **9b, 10b**, *m/z* 777.24 [M+Na], *m/z* 777.24 [M+Na]. (see Supporting Information for CD spectra).

Marfey's Analysis of the Compounds 6 and 10-derived Threonine

Approximately 0.2 mg each of compounds **6** and **10** were separately hydrolyzed with 6N HCl (0.8 mL) overnight in a hot oil bath at 105° C. The hydrolysates were then evaporated to dryness and re-suspended in 0.2 mL H_2O. To each aqueous hydrolysate, 0.5 mg of 1-fluoro-2,4-dinitrophenyl-5-L-leucinamide (*L*-FDLA) suspended in 0.1 mL of acetone and then 20 μL of 1N $NaHCO_3$ were added and the mixtures heated at 40° C for 5 minutes. The mixtures were next cooled to room temperature, neutralized with 2N HCl and evaporated to dryness. The residues were then re-suspended in 500 μL of MeCN and subjected to LC-MS analysis by comparison to standard *D*-threonine and *L*-threonine L-FDLA derivatives that had been prepared in the same fashion. The derivatized threonine residues, derived from compounds **6** and **10**), were found to have identical retention times as the *L*-threonine derivatized standard (*L*-threonine = 19.7 min; *D*-threonine = 22.7min).

Mouse Immunization, cell culturing and cell viability

In order to create a mouse model of allergen induced T_H2 cytokine production suitable for screening, female Balb-C mice age 6–8 weeks, were immunized subcutaneously with 25 μg of ovalbumin (OVA) allergen adsorbed to 1 mg of alum adjuvant in 200 μl phosphate-buffered saline (PBS) weekly for four weeks according to a protocol previously described by our laboratory.[27] At the conclusion of the four-week immunization period, the mice were sacrificed and their spleens surgically removed. Splenocytes were separated through a cell strainer. The splenocytes were then suspended in RPMI-1640 media, centrifuged, and re-suspended in RPMI-1640 media to a concentration of 1.3×10^6 cells/mL and then aliquoted into 96 well plates (100 μL/well). To each test well, containing splenocytes suspended in media, an aliquot of either crude extract, semi-purified extract fractions, or pure compounds suspended in DMSO were added, in addition to an aliquot of stimulating OVA allergen. In addition, replicate wells containing either DMSO or DMSO and OVA allergen were plated as controls. The plates were then incubated for 48 hours during which time the OVA allergen was taken up by the splenocyte antigen presenting cells, and allergen fragments were displayed on the APC surface to stimulate OVA allergen specific T_H2 cells induced to be present in the spleen by the *in vivo* OVA immunization. Control OVA-stimulated splenocytes secrete a variety of cytokines into the supernatant at much higher levels than non OVA-stimulated splenocytes. Adherent splenocytes were stained with trypan blue and counted visually on a hemocytometer to determine cell viability.

Cytokine Quantification

At the end of the splenocyte incubation period, the culture supernatants were removed and cytokine production was quantified using colormetric-based sandwich enzyme linked immunosorbant assays (ELISAs). Mouse IL-1, -5, -13, and TNF-α (R&D Systems) ELISAs were carried out according to the Manufacturer's specifications. Cytokine standards were included in each replicate assay in order to create accurate standard curves.

Supplementary Material

Refer to Web version on PubMed Central for supplementary material.

Abbreviations

T_H2 cells, helper T lymphocytes
IgE, immunoglobulin E
TNF-α, tumor necrosis factor alpha
COSY, two-dimensional correlation spectroscopy
HMBC, heteronuclear multiple bond correlation (spectroscopy)
HRMS, high resolution mass spectroscopy
HR ESI-TOF MS, high resolution electrospray time of flight mass spectroscopy
NOE, nuclear Overhauser enhancement
DMAP, dimethylaminopyridine
CD, circular dichroism
OVA, ova albumin (chicken egg white)
MTPA-Cl, methoxytrifluoromethyphenyl acetic acid chloride

Acknowledgments

This work was a result of financial support from the National Institutes of Health (NIGMS, GMO67557 as part of a T-32 training program in marine biotechnology, and in part by the National Cancer Institute under grant CA44848. The authors express thanks to C. Kauffman for culturing this strain, A. Prieto-Davó, for isolating and identifying this *Streptomyces* strain, K. and S. McElwain and R. Serrano for mouse immunizations and Dr. M. Miller, Dr. J-.Y. Cho

for helpful discussions. We are particularly grateful to Ted Molinski (UCSD) for advice and discussion on applying CD spectral data to the splenocins.

References

1. Ikeda R, Nayar J, Cho JY, Miller M, Rodriguez M, Raz E, Broide DH. Resolution of airway inflammation following ovalbumin challenge. Am. J. Respir. Cell Mol. Biol 2003;28:655–663. [PubMed: 12760963]
2. Itano A, Jenkins M. Antigen presentation to naive CD4 T cells in the lymph node. Nat. Immunol 2003;4:733–739. [PubMed: 12888794]
3. Greenfeder S, Umland SP, Cuss FM, Chapman RW, Egan RW. Th2 cytokines and asthma: the role of interleukin-5 in allergic eosinophilic disease. Respir. Res 2001;2:71–79. [PubMed: 11686868]
4. Wills-Karp M, Chiaramonte M. Interleukin-13 in asthma. Curr. Opin. Pulm. Med 2003;9:21–27. [PubMed: 12476080]
5. Barnes PJ. New drugs for asthma. Nat. Rev. Drug Disc 2004;3:831–844.
6. Salvi SS, Krishna MT, Sampson AP, Holgate ST. The anti-inflammatory effects of leukotriene modifying drugs and their use in asthma. Chest 2001;119:1533–1546. [PubMed: 11348965]
7. Koehn F, Carter GT. The evolving role of natural products in drug discovery. Nat. Rev. Drug Disc 2005;4:206–220.
8. Fenical W, Jensen PR. Developing a new resource for drug discovery: marine actinomycete bacteria. Nat. Chem. Biol 2006;2:666–673. [PubMed: 17108984]
9. Barrow CJ, Oleynek JJ, Marinelli V, Sun HH, Kaplita P, Sedlock DM, Gillum AM, Chadwisk CC, Cooper R. Antimycins, inhibitors of ATP-citrate lyase, from a *Streptomyces* sp. J. Antibiotics 1997;50:729–733. [PubMed: 9360616]
10. Hosotani N, Kumagai K, Nakagawa H, Shimatani T, Saji I. Antimycins A_{10}~A_{16}, seven new antimycin antibiotics produced by *Streptomyces* spp. SPA10191 and SPA-8893. J. Antibiotics 2005;58:460–467. [PubMed: 16161485]
11. Shiomi K, Hatae K, Hatano H, Matsomoto A, Takahashi Y, Jiang C-L, Tomoda H, Kobayashi S, Tanaka H, Omura S. A new antibiotic, antimycin A_9, produced by *Streptomyces* sp. K01-0031. J. Antibiotics 2005;58:74–78. [PubMed: 15813185]
12. Fondja Yao CB, Schiebel M, Helmke E, Anke H, Laatsch H. Prefluostatin and new urauchimycin derivatives produced by *Streptomycete* isolates. Z. Naturforsch 2006;61b:320–325.
13. Ishiyama T, Endo T, Otake N, Yonehara H. Deisovalerylblastmycin produced by *Streptomyces* sp. J. Antibiotics 1976;29:804–808. [PubMed: 993117]
14. Imamura N, Nishijima M, Adachi K, Sano H. Novel antimycin antibiotics, urauchimycins A and B, produced by a marine actinomycete. J. Antibiotics 1992;46:241–246. [PubMed: 8468237]
15. Hayashi K-I, Nozaki H. Kitamycins, new antimycin antibiotics produced by *Streptomyces* sp. J. Antibiotics 1999;52:325–328. [PubMed: 10348050]
16. Ohtani I, Kusumi T, Kashman Y, Kakisawa H. High-field FT NMR application of mosher's method. The absolute configurations of marine terpenoids. J. Am. Chem. Soc 1991;113:4092–4096.
17. Ohkawa S, Fukatsu K, Miki S, Hashimoto T, Sakamoto J, Doi T, Nagai Y, Aono T. 5-Aminocoumarans: dual inhibitors of lipid peroxidation and dopamine release with protective effects against central nervous system trauma and ischemia. J. Med. Chem 1997;40:559–573. [PubMed: 9046347]
18. Kikuchi H, Saito Y, Sekiya J, Okano Y, Saito M, Nakahata N, Kubohara Y, Oshima Y. Isolation and synthesis of a new aromatic compound, brefelamide, from dictyostelium cellular slime molds and its inhibitory effect on the proliferation of astrocytoma cells. J. Org. Chem 2005;70:8854–8858. [PubMed: 16238318]
19. Campbell TW, McCoy VE, Kauer JC, Foldi VS. Preparation of some 9,10-difunctional derivatives of 9,10-dihydro-9,10-ethanoanthracene. J. Org. Chem 1961;26:1422–1426.
20. Fujii K, Ikai Y, Mayumi T, Oka H, Suzuki M, Harada K. A nonempirical method using LC/MS for determination of the absolute configuration of constituent amino acids in a peptide: elucidation of limitations of Marfey's method and of its separation mechanism. Anal. Chem 1997;69:3346–3352.

21. Fujii K, Ikai Y, Oka H, Suzuki M, Harada K. A nonempirical method using LC/MS for determination of the absolute configuration of constituent amino acids in a peptide: combination of Marfey's method and with mass spectrometry and its practical application. Anal. Chem 1997;69:5146–5151.

22. Berova, N.; Nakanishi, K.; Woody, RW. Circular Dichroism Principles and Practice. Vol. 2nd ed.. New York: Wiley-VCH, Inc.; 2000.

23. Kinoshita M, Aburaki S, Umezawa S. Absolute configurations of antimycin lactones and antimycin A. J. Antibiotics 1972;15:373–376. [PubMed: 4649868]

24. Tzung S-P, Kim KM, Basanez G, Giedt CD, Simon J, Zimmerberg J, Zhang KYJ, Hockenbery DM. Antimycin A mimics a cell-death-inducing Bcl-2 homolgy domain 3. Nat. Cell Biol 2001;3:183–191. [PubMed: 11175751]

25. Maeda M, Hasebe Y, Egawa K, Shibanuma M, Nose K. Inhibition of angiogenesis and HIF-1α activity by antimycin A1. Biol. Pharm. Bull 2006;29:1344–1348. [PubMed: 16819166]

26. Kabir AMN, Cao X, Gorog DA, Bassi R, Bellahcene M, Quinlan RA, Davis RJ, Flavell RA, Shattock MJ, Marber MS. Antimycin A induced cardioprotection is dependant on pre-ischemic p38 MAPK activation but independant of MKK3. J. Mol. Cell. Cardiol 2005;39:709–717. [PubMed: 16140323]

27. Broide D, Schwarze J, Tighe H, Gifford T, Nguyen M-D, Malek S, Van Uden JH, Martin-Orozco E, Gelfand EW, Raz E. Immunostimulatory DNA sequences inhibit IL-5, eosinophilic inflammation, and airway responsiveness in mice. J. Immunol 1998;161:7054–7062. [PubMed: 9862743]

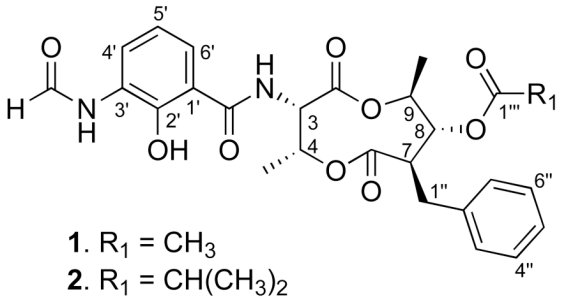

1. $R_1 = CH_3$
2. $R_1 = CH(CH_3)_2$
3. $R_1 = CH(CH_3)CH_2CH_3$

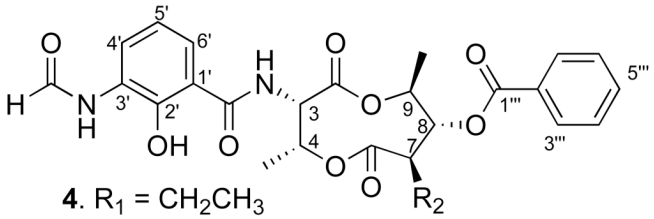

4. $R_1 = CH_2CH_3$
5. $R_2 = CH_2(CH_2)_2CH_3$
6. $R_2 = CH_2(CH_2)_3CH_3$
7. $R_2 = CH_2(CH_2)_4CH_3$
8. $R_2 = CH_2CH(CH_3)(CH_2)_3CH_3$
9. $R_2 = CH_2C_6H_5$

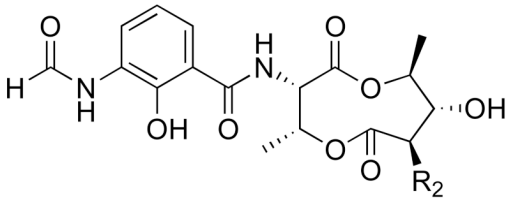

10. $R_2 = CH_2C_6H_5$
11. $R_2 = CH_2(CH_2)_2CH_3$
12. $R_2 = CH_2(CH_2)_3CH_3$
13. $R_2 = CH_2(CH_2)_4CH_3$

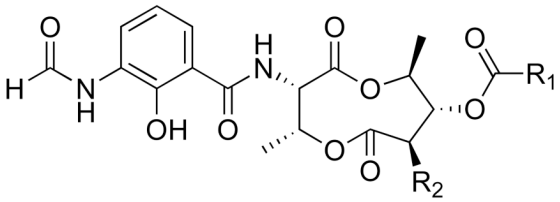

14. $R_1 = CH(CH_3)_2$
$R_2 = CH_2CH_3$
15. $R_1 = CH(CH_3)_2$
$R_2 = CH_2(CH_2)_2CH_3$
16. $R_1 = CH(CH_3)_2$
$R_2 = CH_2CH_2CH(CH_3)_2$
17. $R_1 = CH_2CH_3$
$R_2 = CH_2(CH_2)_4CH_3$

Figure 1.
Structures of **1–10**, and known antimycins **11–17**.

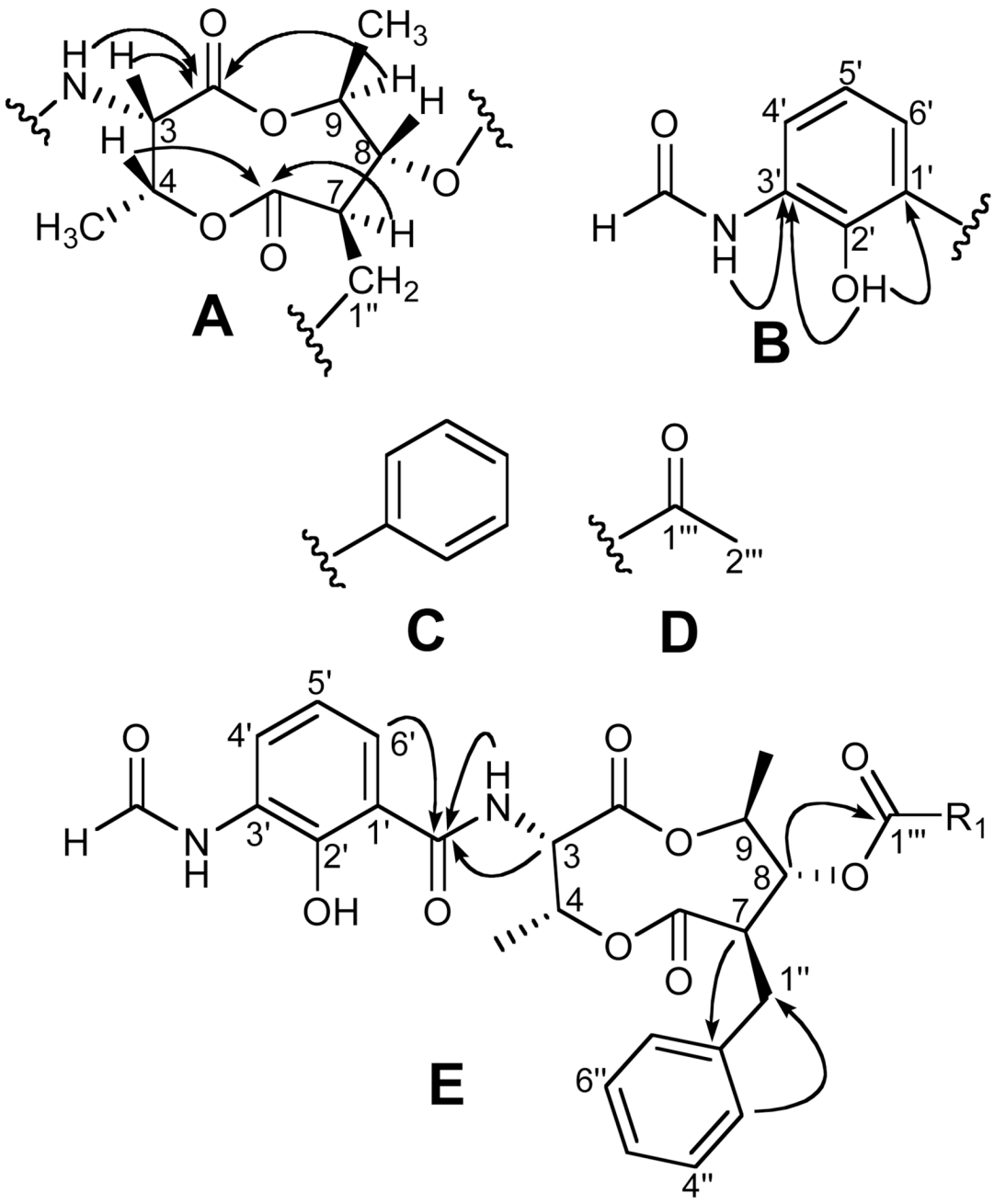

Figure 2.
Substructures with key HMBC correlations used to establish the planar structure of compound **1**.

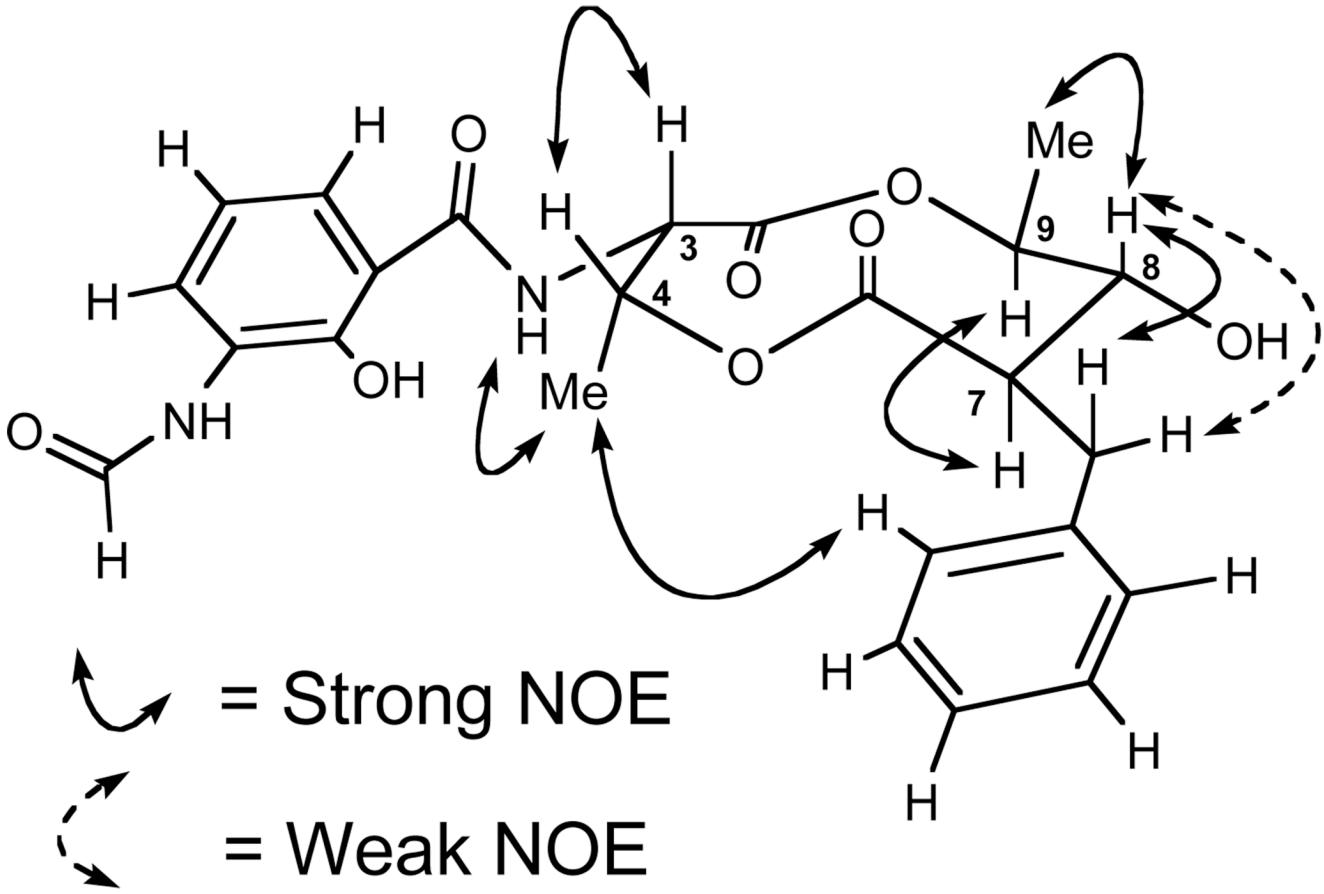

Figure 3.
Key NOESY correlations for establishing the relative configuration of compound **10**.

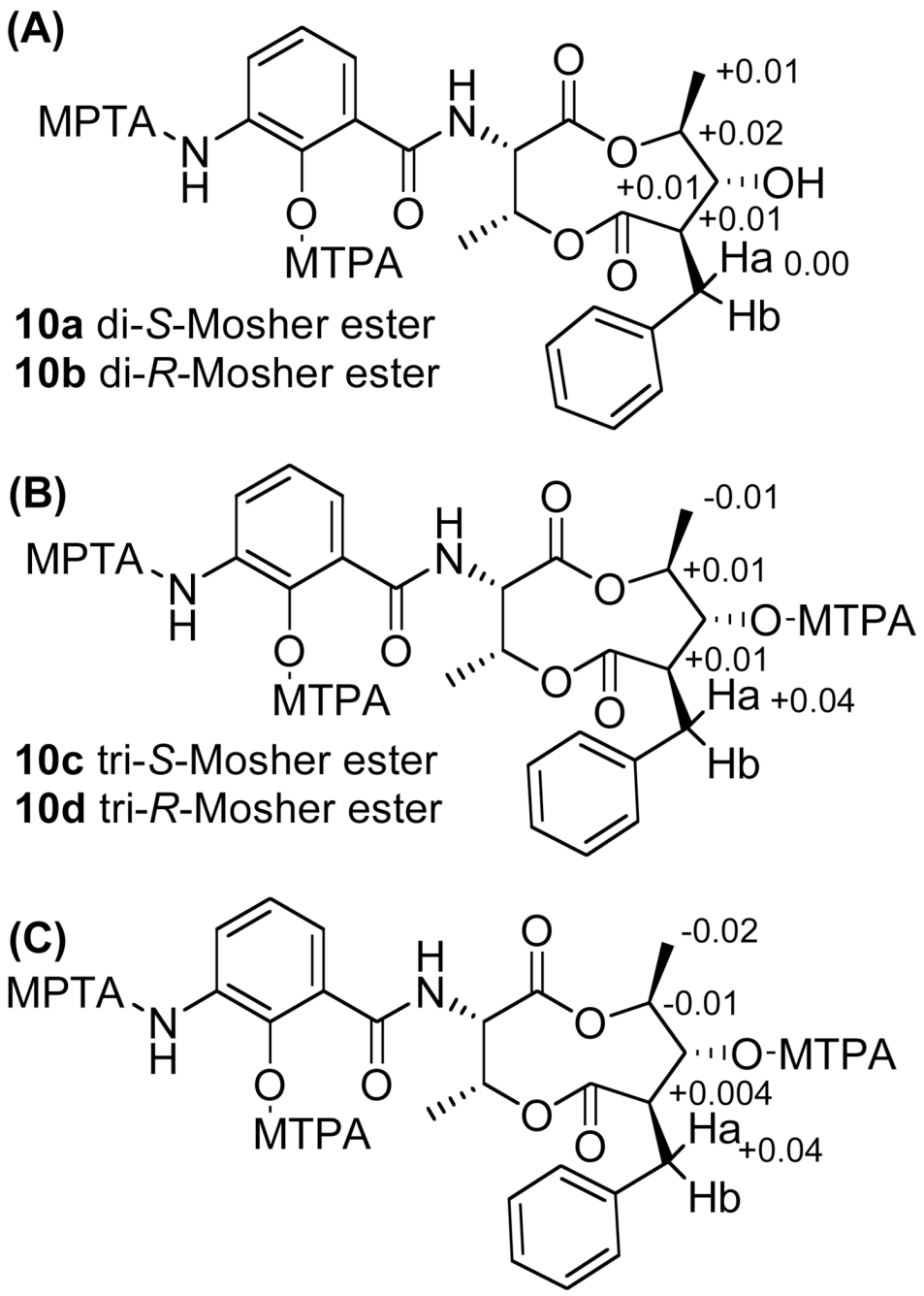

Figure 4.

The structures of derivatives of **10** from Mosher acylation and the differentiation of ^{1}H NMR chemical shift values between *S* and *R* Mosher esters (Δ_{S-R}). (A) compound **10** 2′, 3′-di-Mosher derivatives and Δ_{S-R} values. (B) compound **10** 2′, 3′, 7-tri-Mosher derivatives and Δ_{S-R} values. (C) Tri-Mosher Δ_{S-R} - di-Mosher Δ_{S-R}.

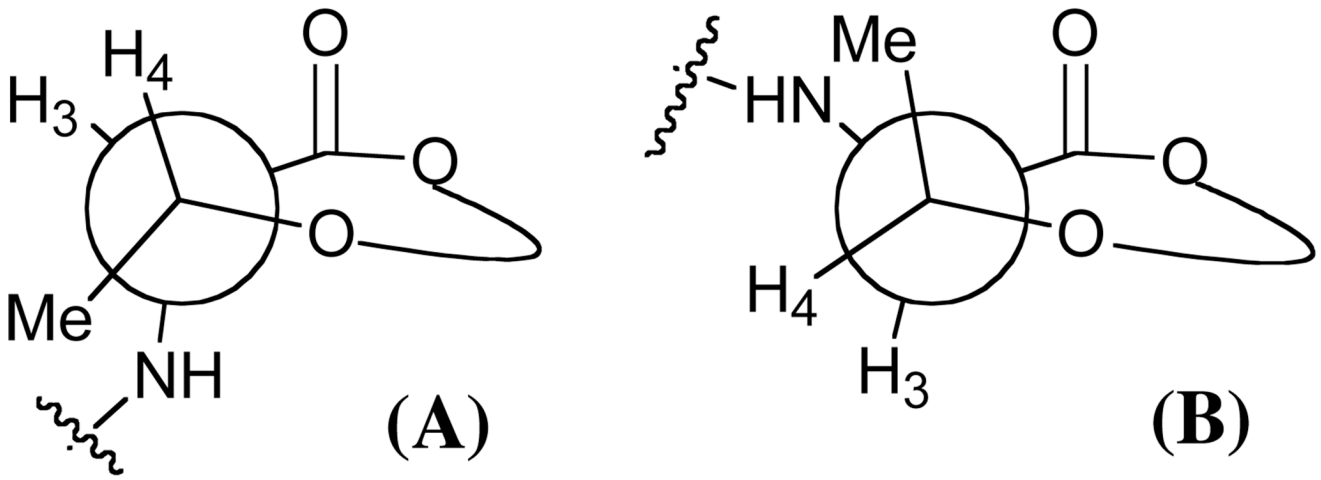

Figure 5.
Orientations of L-(**A**) and D-(**B**) threonine as would be seen with *cis*-relative configurations within the *bis*-lactone ring.

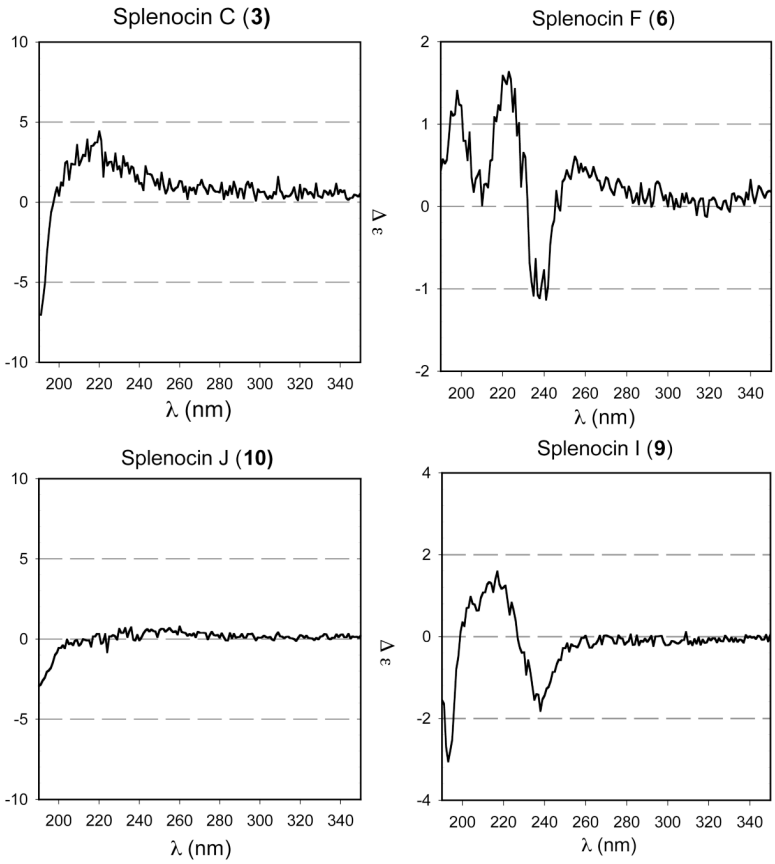

Figure 6.

Representative CD spectra (in MeCN, 22 °C) of splenocin structural groups indicating configuational similarity. Compounds **3** and **10** lack Cotton effects, whereas compounds **6** and **9** show more complex CD spectra.

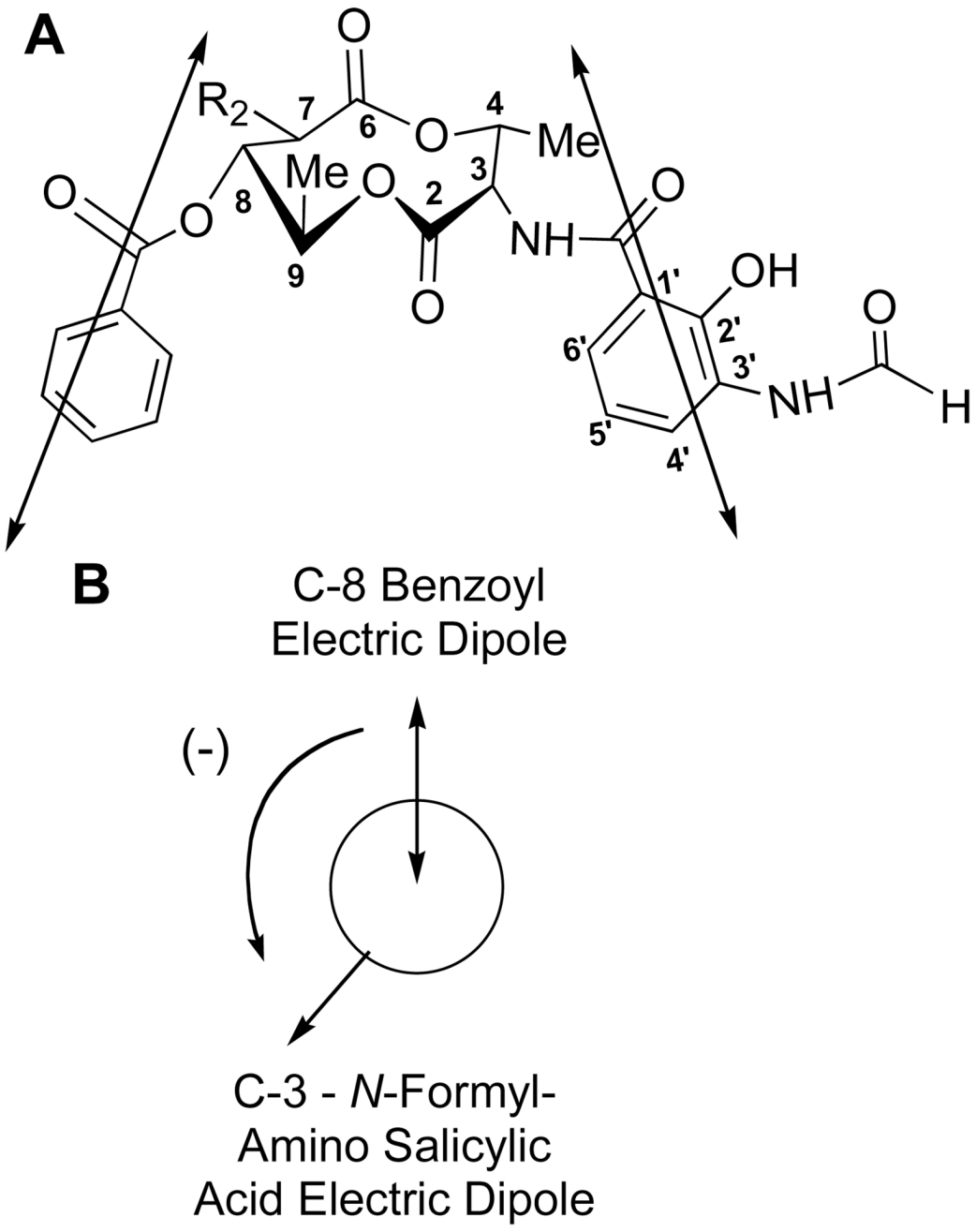

Figure 7.
Three dimensional structure (**A**) and vector diagram (**B**) for compounds **4–9** and **10g** illustrating the confirmation which supports the observed CD Cotton effect.

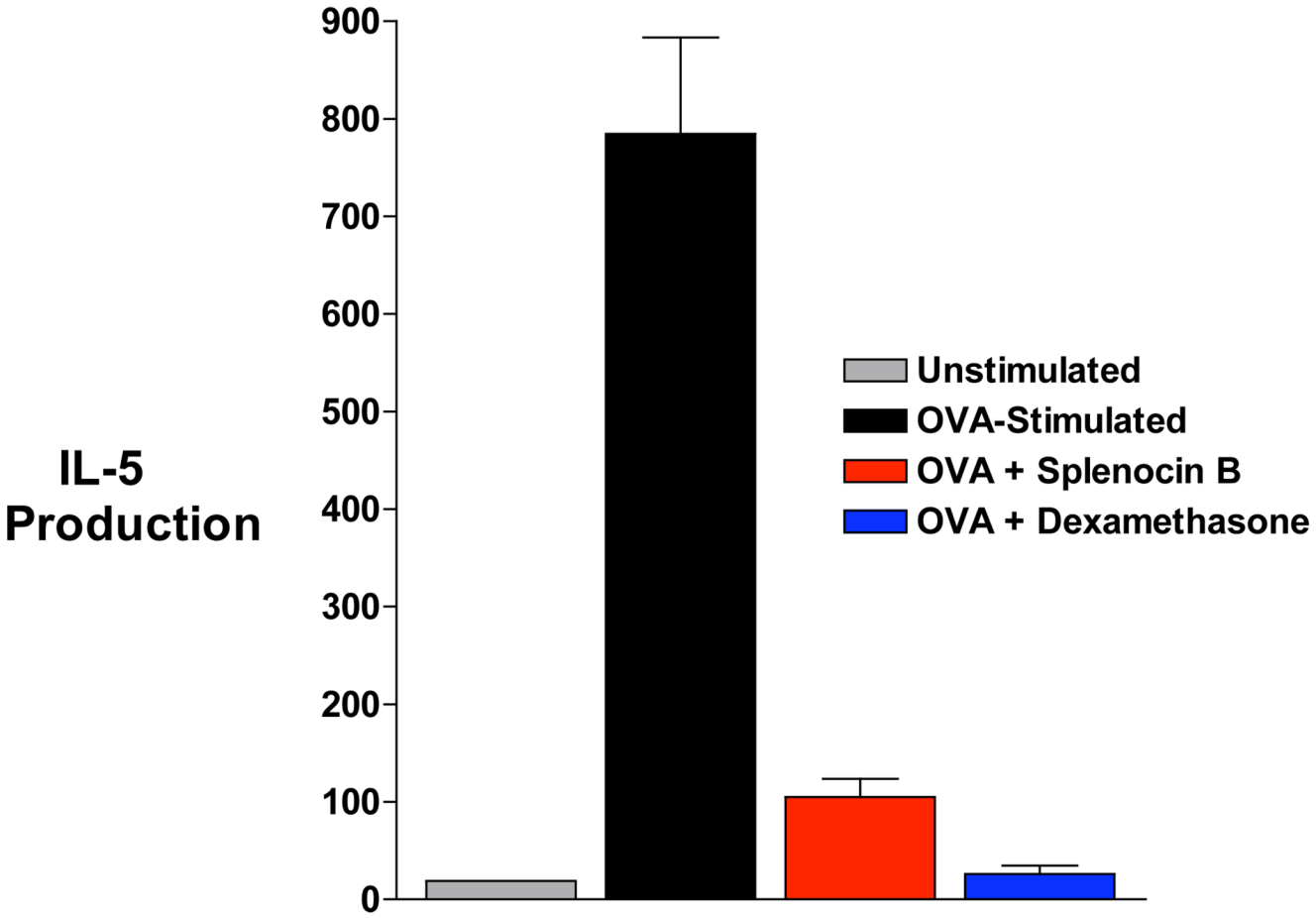

Figure 8.
Interleukin 5 (IL-5) levels of cultured splenocytes. (A) unstimulated control. (B) Ova-stimulated control. (C) Ova-stimulated + compound **2** (5nM). (D) Ova-stimulated + dexamethasone (5 nM).

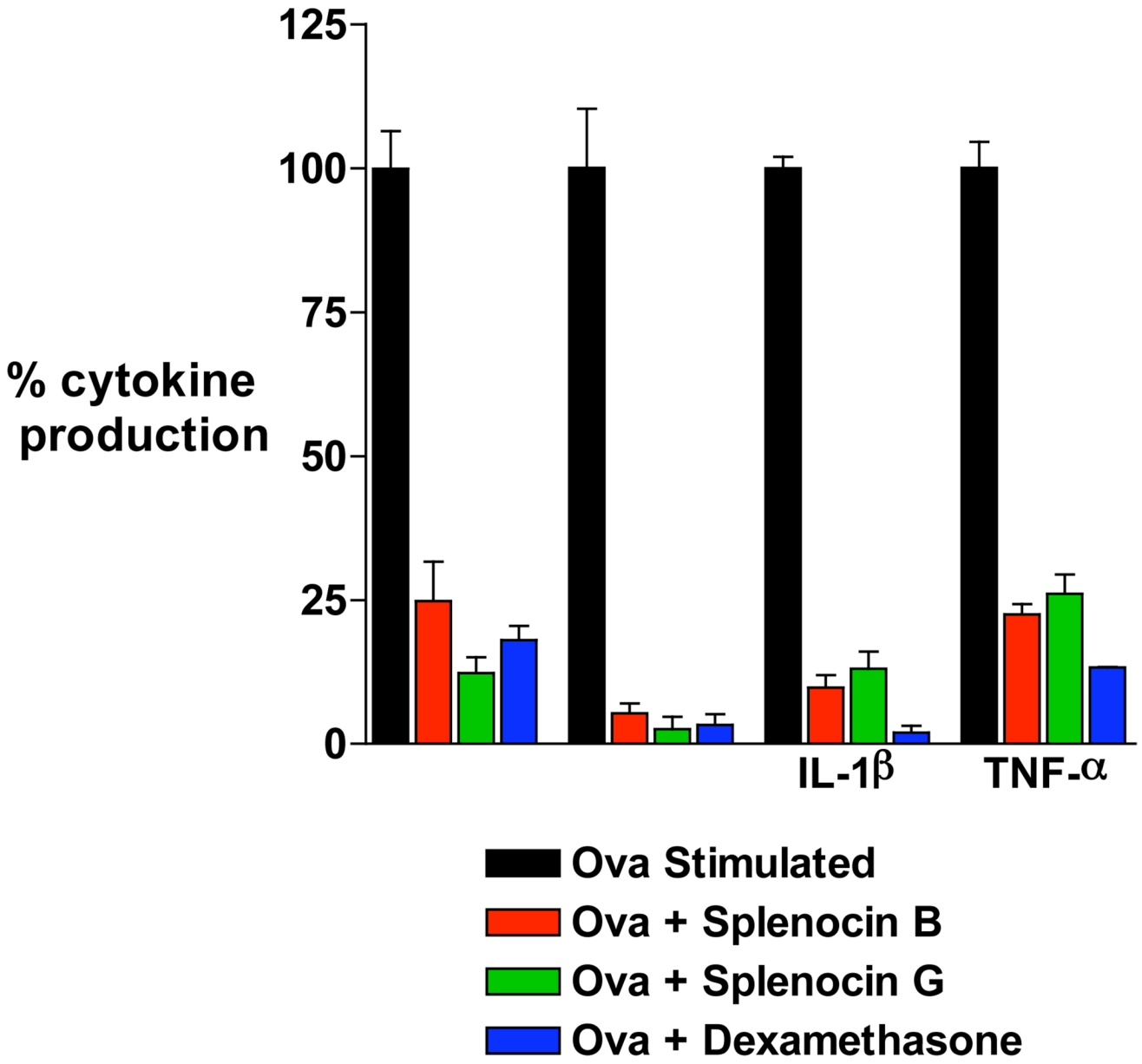

Figure 9.
Splenocyte cytokine inhibition: Levels of T_H2 (IL-5, IL-13) and APC related (IL-1, TNF-α) cytokines of Ova-stimulated splenocytes incubated with either compounds **2** or **7** at 10 nM, or dexamethasone at 10 nM.

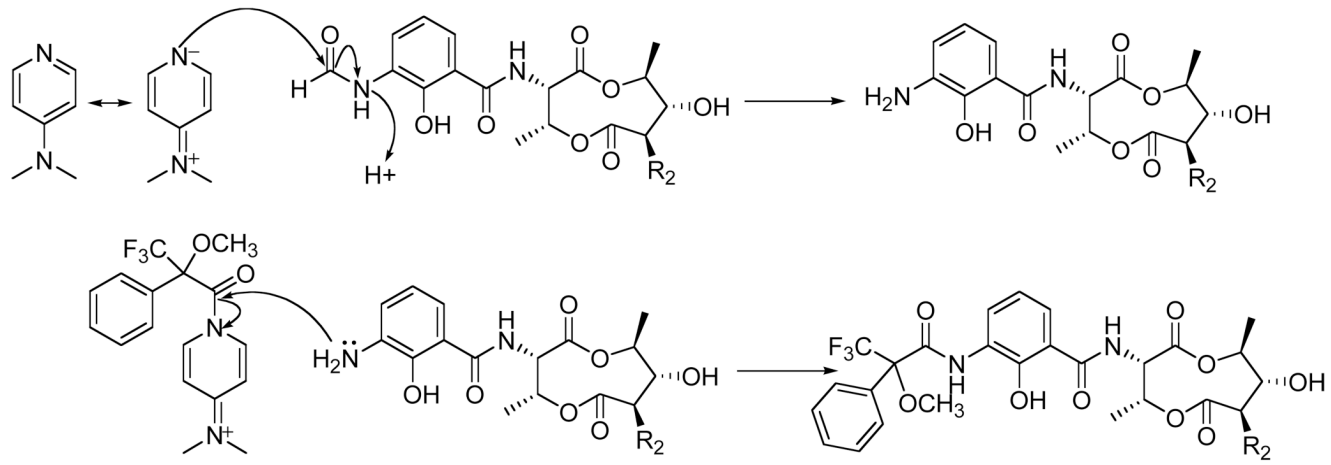

Scheme 1.
Proposed mechanism for deformylation and subsequent acylation of **10**.

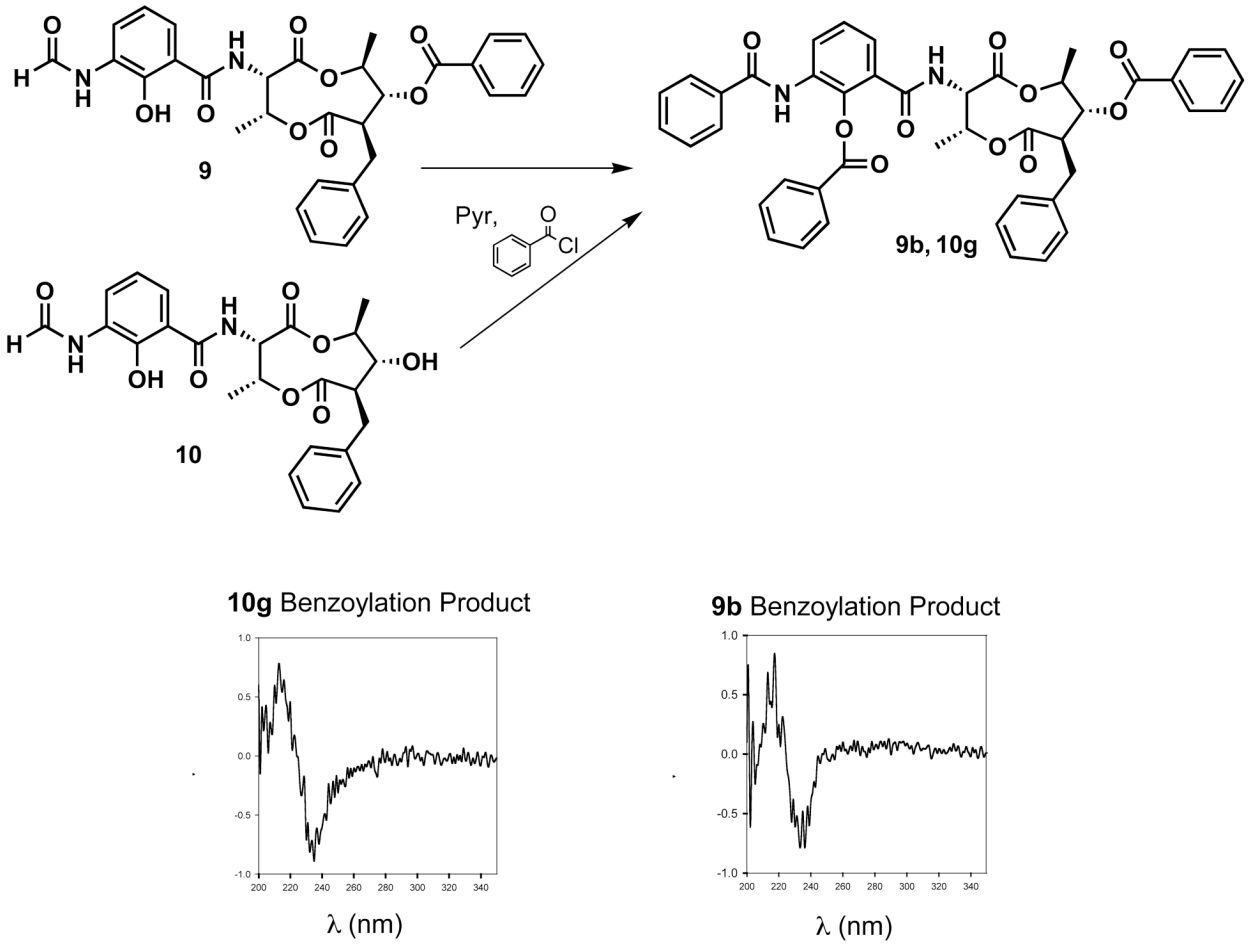

Scheme 2.

Reaction scheme for the benzoylation of compounds **9** and **10** to yield identical tri-benzoylated products (**9b, 10g**) and corresponding CD spectra (in MeCN, 22 °C).

Table 1

NMR spectral data for **1–3** in $CDC1_3$

Position	compound 1		compound 2		compound 3	
	δ_C [a]	δ_H [b] (*J* in Hz)	δ_C [a]	δ_H [b] (*J* in Hz)	δ_C [a]	δ_H [b] (*J* in Hz)
2	170.0		170.1		170.0	
3	53.8	5.24 dd (8.0, 8.0)	53.4	5.26 dd (7.5, 7.5)	53.5	5.25 dd (7.5, 7.5)
4	70.6	5.60 dq (8.0, 6.5)	70.9	5.60 dq (7.5, 7.0)	70.9	5.59 dq (7.5, 7.0)
6	172.8		171.9		172.4	
7	51.6	2.90 ddd (10.5, 10.5, 3.5)	51.9	2.87 ddd (11.5, 10.5, 3.0)	52.0	2.87 ddd (10.5, 10.5, 3.5)
8	75.6	5.19 t (10.5)	75.0	5.20 t (10.5)	75.1	5.21 t (10.5)
9	75.0	5.01 m	74.7	5.01 m	74.8	5.00 m
4-Me	15.0	1.16 d (6.5)	14.7	1.15 d (7.0)	14.7	1.14 br d (7.0)
9-Me	18.0	1.32 d (6.5)	17.8	1.31 d (6.5)	17.9	1.31 d (6.5)
1′	112.5		112.6		112.5	
2′	150.6		150.7		150.6	
3′	127.7		127.4		127.4	
4′	124.9	8.52 d (7.5)	124.8	8.52 d (7.5)	124.8	8.51 d (8.0)
5′	119.0	6.89 t (7.5)	118.8	6.89 t (7.5)	119.0	6.88 t (7.5)
6′	120.2	7.20 d (7.5)	120.3	7.18 d (7.5)	120.0	7.18 d (8.0)
1′-CONH	169.5		169.3		169.3	
1′-CONH		6.98 d (8.0)		7.03 d (7.5)		6.98 d (8.0)
2′-OH		12.59 br s		12.62 br s		12.60 br s
3′-NHCHO		7.87 br s		7.94 s		7.89 br s
3′-NHCHO	159.5	8.48 s	159.1	8.47 s	158.9	8.49 s
1″	34.7	2.97 dd (13.5, 10.5)	34.5	2.97 dd (13.5, 11.5)	34.5	2.97 dd (13.0, 10.5)
		2.71 dd (13.5, 3.5)		2.68 dd (13.5, 3.5)		2.70 dd (13.5, 3.5)
2″	138.5		137.9		137.9	
3″	128.8	7.12 d (8.0)	128.7	7.11 d (8.0)	128.7	7.11 d (8.0)
4″	128.6	7.24 t (8.0)	128.5	7.24 t (8.0)	128.6	7.24 t (8.0)
5″	126.6	7.18 t (8.0)	126.6	7.17 t (8.0)	126.6	7.18 t (8.0)
6″	128.6	7.24 t (8.0)	128.5	7.24 t (8.0)	128.6	7.24 t (8.0)
7″	128.8	7.12 d (8.0)	128.7	7.11 d (8.0)	128.7	7.11 d (8.0)
1‴	170.2		175.7		175.3	

Position	compound 1		compound 2		compound 3	
	δ_C [a]	δ_H [b] (*J* in Hz)	δ_C [a]	δ_H [b] (*J* in Hz)	δ_C [a]	δ_H [b] (*J* in Hz)
2‴	20.9	2.04 s	34.1	2.59 m	41.3	2.43 m
3‴			18.9	1.22 d (7.0)	26.5	1.75 m
						1.53 m
4‴					11.8	0.95 t (7.5)
5‴					16.7	1.20 d (7.5)

[a] Assignment by ^{13}C, HSQC, and HMBC NMR methods at 125 MHz.

[b] Assignment by ^{1}H, gHSQC, and gHMBC NMR methods at 500MHz.

Table 2

NMR spectral data for **4–8** in $CDCl_3$.

Position	compound 4		compound 5		compound 6	
	δ_C [a]	δ_H [b] (*J* in Hz)	δ_C [a]	δ_H [b] (*J* in Hz)	δ_C [a]	δ_H [b] (*J* in Hz)
2	170.5		170.1		170.1	
3	53.9	5.32 dd (8.0, 7.5)	53.7	5.30 dd (8.0, 7.5)	53.9	5.30 dd (8.0, 7.0)
4	71.2	5.76 dq (7.5, 7.0)	71.0	5.76 dq (7.5, 6.5)	71.3	5.75 dq (7.5, 7.0)
6	172.6		172.9		172.9	
7	52.0	2.62 ddd (10.0, 10.0, 3.0)	50.2	2.68 ddd (10.0, 10.0, 3.0)	50.2	2.65 ddd (10.0, 10.0, 3.0)
8	76.4	5.33 t (10.0)	76.3	5.32 t (10.0)	76.5	5.32 t (10.0)
9	75.0	5.15 m	75.0	5.14 m	75.2	5.14 m
4-Me	15.2	1.32 [d] d (7.0)	15.0	1.33 d [d] (6.5)	15.0	1.33 [d] d (7.0)
9-Me	18.0	1.33 [d] d (6.5)	17.9	1.32 d [d] (6.5)	17.9	1.33 [d] d (7.0)
1′	112.7		112.5		112.5	
2′	151.0		150.6		150.6	
3′	127.0		127.4		127.4	
4′	124.8	8.54 d (8.0)	124.8	8.54 d (8.0)	124.8	8.53 d (8.0)
5′	119.2	6.91 t (8.0)	120.1	6.91 t (8.0)	119.4	6.90 t (8.0)
6′	120.3	7.23 m[c]	120.8	7.23 m[c]	120.4	7.23 m[c]
1′-CONH	169.0		169.4		169.4	
1′-CONH		7.08 d (8.0)		7.07 d (8.0)		707 d (8.0)
2′-OH		12.60 s		12.60 s		12.60 s
3′-NHCHO		7.91 br s		7.92 s		7.92 s
3′-NHCHO	159.0	8.49 s	158.9	8.49 s	158.9	8.49 s
1″a	21.8	1.75 m	28.2	1.76 m	28.2	1.76 m
1″b		1.50 m[c]		1.40 m		1.40 m
2″	11.5	0.86 t (8.0)	29.3	1.15 m	36.5	1.08 m
				1.24 m		
3″			22.3	1.23 m	26.5	1.45m
4″			13.8	0.80 t (7.0)	22.3	0.77[d] d (7.0)
5″					22.3	0.78[d] d (7.0)
6″						
7″						

Position	compound 4		compound 5		compound 6	
	δ_C [a]	δ_H [b] (*J* in Hz)	δ_C [a]	δ_H [b] (*J* in Hz)	δ_C [a]	δ_H [b] (*J* in Hz)
1‴	165.5		165.2		165.2	
2‴	129.0		129.0		129.0	
3‴	130.0	8.04 d (8.0)	129.9	8.05 d (8.0)	129.9	8.04 d (7.5)
4‴	128.7	7.47 t (8.0)	128.7	7.47 t (8.0)	128.7	7.47 t (7.5)
5‴	133.8	7.61 t (8.0)	133.7	7.61 t (8.0)	133.9	7.63 t (7.5)
6‴	128.7	7.47 t (8.0)	128.7	7.47 t (8.0)	128.7	7.47 t (7.5)
7‴	130.0	8.04 d (8.0)	129.9	8.05 d (8.0)	129.9	8.0 d (7.5)

[a] Assignment by 1-D ^{13}C methods at 125 MHz.

[b] Assignment by ^{1}H, gHSQC, and gHMBC NMR methods at 500 MHz.

Table 3

NMR spectral data for **9** and **10** in $CDCl_3$.

	compound 9		compound 10	
Position	δ_C [a]	δ_H [b] (*J* in Hz)	δ_C [a]	δ_H [b] (*J* in Hz)
2	170.1		170.1	
3	53.6	5.29 dd (8.0, 7.5)	53.5	5.21 dd (7.5, 7.0)
4	71.0	5.64 dq (7.5, 7.0)	70.7	5.58 dq (7.5, 7.0)
6	172.0		173.0	
7	52.0	3.06 dt (10.0, 10.0)	54.0	2.69 ddd (10.5, 10.0, 3.5)
8	76.1	5.45 t (10.0)	77.3	3.73 dt (10.0, 10.0)
9	74.9	5.12 m	76.9	4.87 dq (10.0, 10.0)
8-OH				1.62 br s
4-Me	14.8	1.18 d (6.5)	14.7	1.15 d (7.0)
9-Me	18.0	1.37 d (6.5)	18.4	1.47 d (6.0)
1′	112.5		112.5	
2′	150.6		150.6	
3′	127.4		127.3	
4′	124.7	8.52 d (8.0)	124.8	8.51d (8.0
5′	119.0	6.89 t (8.0)	119.0	6.88 t (8.0)
6′	120.0	7.19 t (8.0)	120.1	7.18 d (8.0)
1′-CONH	169.4		169.3	
1′-CONH		7.01 br d (8.0)		7.01 d (7.5)
2′-OH		12.6 br s		12.6 s
3′-NHCHO		7.88 br s		7.87 br s
3′-NHCHO	158.9	8.48 s	159.0	8.47 s
1″a	34.7	3.06 dd (20.0, 10.0)	35.1	3.19 dd (13.5, 3.5)
1″b		2.78 dd (20.0, 10.0)		2.98 dd (13.5, 10.5)
2″	137.8		138.4	
3″	128.7	7.09 d (7.5)	126.6	7.17 d (7.5)
4″	128.5	7.19 t (7.5)	128.6	7.26 t (7.5)
5″	126.6	7.13 t (7.5)	128.8	7.16 t (7.5)
6″	128.5	7.19 t (7.5)	128.6	7.26 t (7.5)
7″	128.7	7.09 d (7.5)	126.6	7.17 d (7.5)
1‴	165.3			
2‴	129.0			
3‴	129.9	8.05 d (8.0)		
4‴	128.7	7.48 t (8.0)		
5‴	133.9	7.62 t (8.0)		
6‴	128.7	7.48 t (8.0)		
7‴	129.9	8.05 d (8.0)		

[a] Assignment by ^{13}C, HSQC, and HMBC NMR methods at 125 MHz.

[b] Assignment by ^{1}H, gCOSY, gHSQC, and gHMBC NMR methods at 500 MHz.

Table 4

Coupling constant values for key protons on the *bis*-lactone ring.

	$^3J_{H3\text{-}H4}$	$^3J_{H7\text{-}H8}$	$^3J_{H8\text{-}H9}$
compounds **1–3**	7.5 Hz	10.5 Hz	10.5 Hz
compounds **4–8**	7.5 Hz	10.0 Hz	10.0 Hz
compound **9**	7.5 Hz	10.0 Hz	10.0 Hz
compound **10**	7.5 Hz	9.0 Hz	9.0 Hz
compound **17**	7.5 Hz	10.0 Hz	10.0 Hz

Table 5

Compounds **1–10** and dexamethasone (IC50 values) for inhibition of T_H2 cytokines IL-5 and IL-13 production, and cytotoxicity (LD50 values).

	IL-5 IC50 nM	IL-13 IC50 nM	Cytotoxicity LD50 nM
Dexamethasone	5±0.1	5±0.1	>7100
compound **1**	3.1 ± 1.2	not available	>1800
compound **2**	1.8 ± 0.2	1.6 ± 0.02	>1700
compound **3**	6.7 ± 0.2	7.3 ± 4.2	>560
compound **4**	47.9 ± 2.9	43.7 ± 3.5	>550
compound **5**	16.6 ± 1.8	15.9 ± 1.1	>570
compound **6**	9.4 ± 2.8	6.8 ± 0.3	>560
compound **7**	5 ± 0.4	5.2 ± 0.1	>550
compound **8**	4.3 ± 0.5	5.1 ± 0.1	>1600
compound **9**	15.8 ± 1.0	15.2 ± 1.3	>540
compound **10**	1022.7 ± 52.3	826.3 ± 187.6	>6000